Gravitational Waves from Neutron Star Magnetic Explosions

Emily Kuhn, Brynmor Haskell, Andrew Melatos, Paul Lasky, Patrick Clearwater

August 11, 2015

Abstract

The detection of gravitational waves is one of the most anticipated events in modern science. Postulated by Albert Einstein in his 1915 Theory of Gravity, these phenomena are thought to hold important insights into the workings and origin of our universe. Many sources of gravitational wave signals are being explored in an effort towards first detection, one of these being highly magnetic neutron stars known as magnetars. We use the numerical code PLUTO to simulate magnetars and their development over Alfven time scales, in order to determine whether they have potential to produce detectable signals. We investigate two field configurations and their evolutions, finding that the wave strain produced is sufficient to make certain neutron stars candidates for LIGO.

1 Introduction

1.1 Gravitational Waves

Albert Einstein first postulated gravitational waves as part of his theory of gravity. Gravitational waves, as we understand them, arise when a massive body undergoes an acceleration, provided the motion is not spherically or cylindrically symmetric, and are the result of a time varying quadrupole. These waves are in the form of three types of signals:

1. Inspirals, which describe a signal increasing in frequency as two objects coalesce, such as from a system

of binary black holes or neutron stars

2. Bursts, which characterize a short non-repeating signal, and are the product of such things as supernovae explosions

3. Continuous Signals, which are steady and consistent and from such sources as rotating asymmetric stars.

Though gravitational waves are no challenge to produce, detection is far from trivial. For one, their wavelengths are on the order of kilometers long, requiring interferometers that are also kilometers long for detection. Additionally, the amplitudes of the strongest signals we expect to observe on Earth will have a parameter "wave strain" (h), which describes the amplitude, at $h = 10^{-20}$ or less. "This is enough to distort the shape of the Earth by 10-13 metres, or about 1% of the size of an atom. By contrast, the (nonradiative) tidal field of the Moon raises a tidal bulge of about 1 meter on the Earth's oceans."(Caltech). Clearly, these signals are so weak that it would take an extraordinarily dramatic event, such as the collision of two black holes, to produce something detectable with our current apparatuses.

Gravity has many interesting properties, reaching far beyond what was originally formulated by Newton. "...According to Einstein's general theory of relativity, [gravity] is how mass deforms the shape of space. Einstein realized that the deformation can propagate throughout the Universe. If you could watch a gravitational wave head-on as it moves toward you, you would see it alternately stretching and compressing space, in the updown and leftright directions." (Nature).

The detection of these waves would be important for science in several respects. For one, it would confirm Einstein's theory of gravity, which, while universally accepted as the formalism that governs large massive bodies, lacks this critical experimental verification. More importantly, being able to detect gravitational waves will open up a new medium through which we can image the universe. This is particularly interesting because gravitational waves can pass through barriers unaltered, whereas light, our main method of viewing the universe, would be scattered. This will allow us to see parts of the Universe that were previously invisible, such as the interiors of stars.

We will now investigate where these gravitational waves arise mathematically.

To show how gravitational plane waves arise mathematically, we look to the weak-field approximation,

in which we decompose our metric into the flat minkowsi metric and a small perturbation.

$$g_{\mu\nu} = \eta_{\mu\nu} + h_{\mu\nu} \tag{1}$$

We assume $|h_{\mu\nu}| << 1$, so we can ignore terms O(h^2). From here we obtain the equation

$$g^{\mu\nu} = \eta^{\mu\nu} - h^{\mu\nu} \tag{2}$$

We must compute connection coefficients, for they will be necessary to calculate our tensors:

$$\Gamma^{\rho}_{\mu\nu} = \frac{1}{2} g^{\rho\lambda}(g_{\mu\lambda,\nu} + g_{\nu\lambda,\mu} - g_{\mu\nu,\lambda}) = \frac{1}{2}\eta^{\rho\lambda}(h_{\mu\lambda,\nu} + h_{\nu\lambda,\mu} - h_{\mu\nu,\lambda}) \tag{3}$$

Computing our Riemann, Ricci and thus Einstein Tensors, we obtain:

Riemann Tensor:

$$R_{\mu\nu\rho\sigma} = \frac{1}{2}\left(\partial_\rho\partial_\nu h_{\mu\nu} + \partial_\sigma\partial_\mu h_{\nu\rho} - \partial_\sigma\partial_\nu h_{\mu\rho} - \partial_\rho\partial_\mu h_{\nu\sigma}\right) \tag{4}$$

Ricci Tensor:

$$R_{\mu\nu} = \frac{1}{2}\left(\partial_\sigma\partial_\nu h^{\sigma}_{\mu} + \partial_\sigma\partial_\mu h^{\sigma}_{\nu} - \partial_\mu\partial_\nu h - \Box h_{\mu\nu}\right) \tag{5}$$

Where $\Box = -\partial_t^2 + \partial_x^2 + \partial_y^2 + \partial_z^2$

Einstein Tensor:

$$G_{\mu\nu} = R_{\mu\nu} - \frac{1}{2}\eta_{\mu\nu}R = 8\pi G T_{\mu\nu} \tag{6}$$

In our weak field approximation, $g_{\mu\nu} = \eta_{\mu\nu} + h_{\mu\nu}$ is not uniquely defined– our perturbation can be different in other coordinate systems. To address this and eliminate degeneracy, we must fix a gauge. In this case we will be choosing the transverse gauge, which is analogous to the Coulomb gauge in electromagnetism.

We write $h_{\mu\nu}$ as a decomposition of its trace and trace-free parts:

$$h_{00} = -2\Phi \tag{7}$$

$$h_{0i} = \omega_i \tag{8}$$

$$h_{ij} = 2s_{ij} - 2\psi\delta_{ij} \tag{9}$$

In this gauge, our Einstein tensor becomes:

$$G_{00} = 2\nabla^2\psi = 8\pi G T_{00} \tag{10}$$

In weak field limit, we take $T_{\mu\nu} = 0$. We obtain the equations $\nabla^2\psi = 0$, $\nabla^2\omega_j = 0$, $\nabla^2\phi = 0$, $\Box s_{ij} = 0$

We now have our transverse traceless gauge: $h^{TT}_{\mu\nu} = \begin{pmatrix} 0 & 0 & 0 & 0 \\ 0 & 0 & 0 & 0 \\ 0 & 0 & 2s_{ij} & 0 \\ 0 & 0 & 0 & 0 \end{pmatrix}$.

We use $h^{TT}_{\mu\nu}$ for its convenience when comparing with other resources. It is purely spacial, traceless and transverse. Our equation of motion is then

$$\Box h^{TT}_{\mu\nu} = 0 \tag{11}$$

and it follows that

$$\partial_\mu h^{\mu\nu}_{TT} = 0. \tag{12}$$

It is from this equation that our plane wave solutions arise. Looking at equation 12, we see that a solution is

$$h^{TT}_{\mu\nu} = C_{\mu\nu} e^{ik_\sigma x^\sigma} \tag{13}$$

where $C_{\mu\nu}$is a constant, symmetric and purely spacial tensor, and $k^\sigma = \left(\omega, k^1, k^2, k^3\right)$ is the wave vector. By plugging our solution back into the equation of motion, we obtain the condition $k_\sigma k^\sigma = 0$, which tell us that the plane wave is a solution if the wave vector is null. To ensure that our perturbation is transverse, we require

$$0 = \partial_\mu h^{\mu\nu}_{TT} = iC^{\mu\nu} k_\mu e^{ik_\sigma x^\sigma} \tag{14}$$

so,

$$0 = C^{\mu\nu} k_\mu. \tag{15}$$

To simplify our solution, let's consider a wave traveling in the x^3 direction:

$$k^\sigma = \left(\omega, 0, 0, k^3\right) = (\omega, 0, 0, \omega)\,. \tag{16}$$

We can determine that $k^3 = \omega$ because our wave vector is null. We can from there derive that $C_{3\nu} = 0$ and thus that the only non-zero components of our symmetric, traceless $C_{\mu\nu}$ are C_{11}, $-C_{11}$, C_{12} and C_{21}. Thus,

we see in general that

$$C_{\mu\nu} = \begin{pmatrix} 0 & 0 & 0 & 0 \\ 0 & C_{11} & C_{21} & 0 \\ 0 & C_{12} & -C_{11} & 0 \\ 0 & 0 & 0 & 0 \end{pmatrix} .$$

This tells us that for a plane wave in this transverse gauge, only two components (outside of the frequency), C_{11} and C_{12} characterize the plane wave behavior. Now that we better understand the mathematical origins of gravitational plane waves, we will discuss the research being done to detect them.

1.2 LIGO

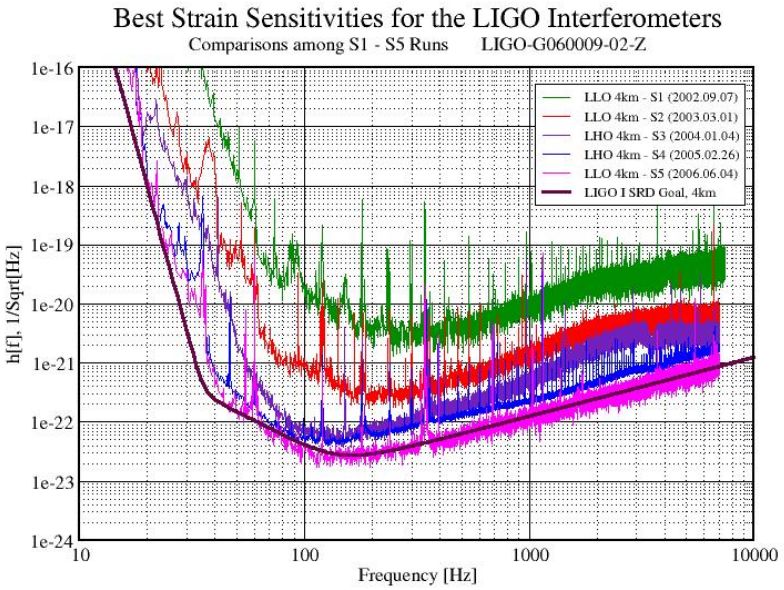

Figure 1: Here, the strain sensitivity of LIGO is shown as a function of frequency. (https://www.advancedligo.mit.edu/summary.html)

The Laser Interferometer Gravitational-Wave Observatory, or LIGO, is one of the leading collaborations

in the gravitational wave hunt. The LIGO experiment uses a pair of ground based interferometers in the United States, one in Livingston, Louisiana and the other in Hanford, Washington to isolate correlated signals, some of which they hope to identify as originating from gravitational waves. The mirrors are 11kg, the arms 4km long and the laser is powered at 10 Watts. LIGO can measure frequencies between 10Hz and 10,000Hz and a wave strain (h) of roughly $10^{-}23$(LIGO).

With the introduction of advanced LIGO in Fall of 2015, the laser power will increase to 200 W, the test mass objects will be almost one third larger in diameter, and the frequency cutoff will move from 40Hz down to 10Hz.The observable volume of space of advanced LIGO is 1000 times greater than that of initial LIGO, allowing better access to potential sources (MIT).

2 Magnetic Fields in Neutron Stars

2.1 Magnetic Field Stability in Ap/Bp Stars

Ap, Bp stars are peculiar A and B stars which have an abundance of certain metals and a much slower rotation than typical A, B stars. They have large magnetic fields ranging from 0.03-3 tesla. Several models of these stars have been created, though they fail to describe many of our observations accurately, which suggests that they have a complex field structure. Much of the work on stable fields in these stars comes from Dr. Jonathan Braithwaite, who uses numerical simulations to look at stability of Ap stars on Alfven time scales, or the time scale on which a magnetic wave crosses a star.

To examine field configurations and features in these types of stars, the procedure followed is generally the same: begin with some reasonable initial state based on what is known from observation and time evolve it numerically. If we see the magnetic field settle into a stable configuration after several Alfven time scales, it is considered stable. By this method, the same stable field configuration is always found: a nearly asymmetrical torus inside the star with toroidal and poloidal components of comparable strength. The torus can be either right or left handed depending on initial conditions. These general configurations are not affected by initial conditions, but the surface field strength does depend on them.

Much of the work done on fields in Ap and Bp stars can be applied to highly magnetized neutron stars,

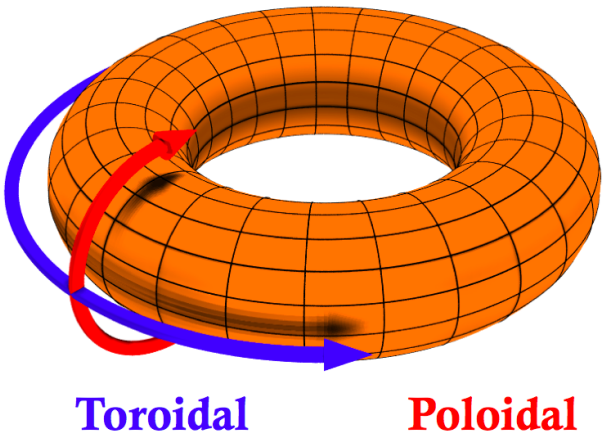

Figure 2: Stable magnetic fields have both toroidal and poloidal components.

which have exciting applications to gravitational wave detection.

2.2 Neutron Stars and Magnetars

Neutron stars are some of the most dramatic phenomena in our universe. With a radius on the order of 10km, they can be twice as massive as our sun. Magnetars are highly magnetic neutron stars, with fields that can reach above 10^{15} Gauss. This is particularly impressive when one considers that the magnetic field of the Earth is under 1 Gauss. These strong magnetic fields deform the star as a result of the Lorentz forces they exert

$$\vec{F}_{Lorentz} = q\vec{v} \times \vec{B}. \tag{17}$$

Energy is released by some form of rearrangement of the magnetic field configuration in the star. These magnetic fields were probably already present at birth. They release energy over a timescale of around 10^4 years, which is much greater than the Alfven time scale over which unstable fields evolve (0.1s). They have ample time to either evolve into a stable configuration or decay to nothing before being frozen in by the crust. In general, it has been found that an arbitrary unstable initial field does not decay completely, but gets stuck in a stable equilibrium at some magnitude (Braithwaite and Nordlund 2006).

For gravitational wave detection it is important to know what the magnetic field configuration in a neutron star is. If the magnetic and rotational axes are not aligned, the deformation due to the magnetic

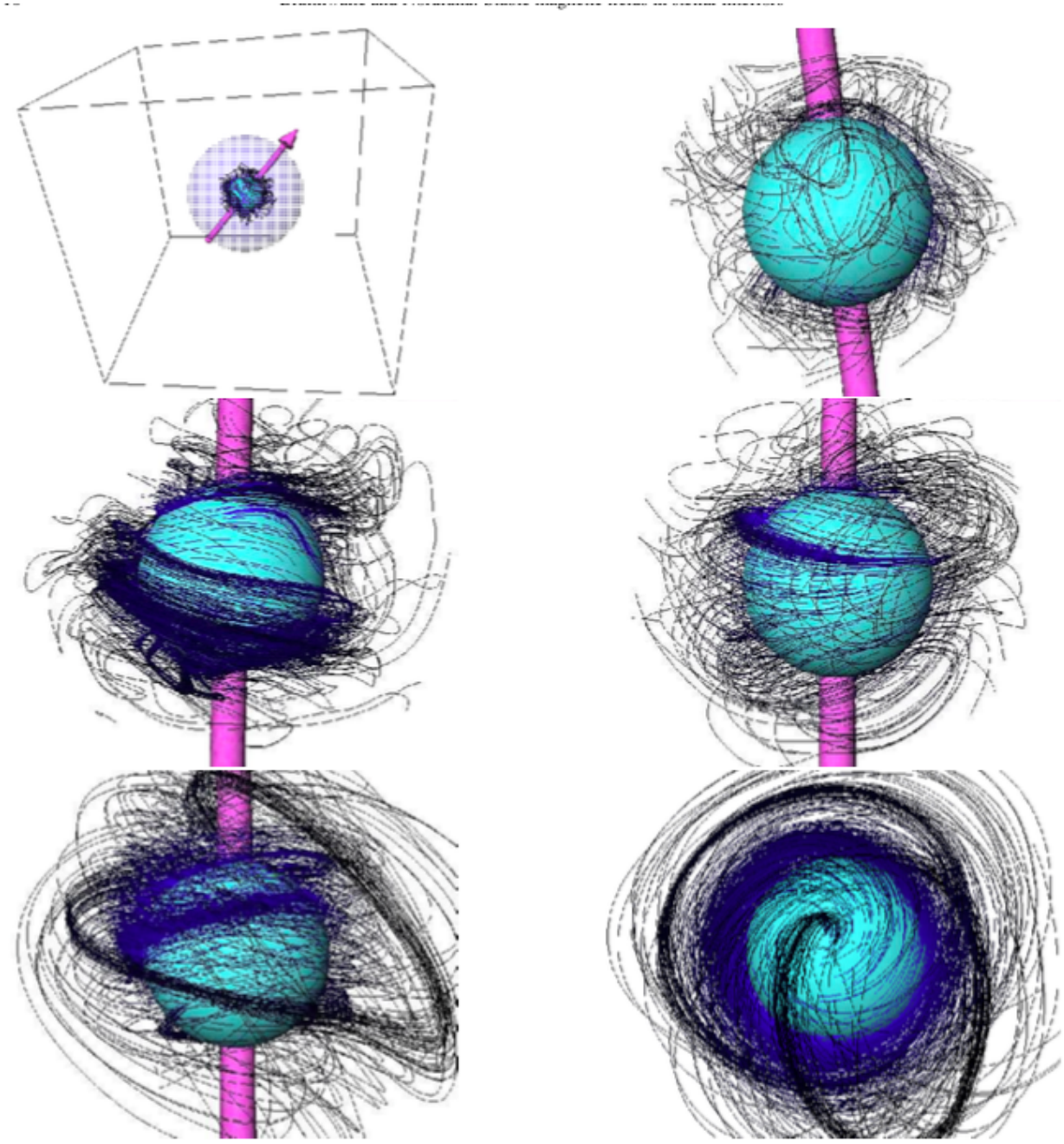

Figure 3: The evolution of a magnetic field in a stable Ap star at times t = 0 days (top row figures) 0.18 days (middle left figure), 0.54 days (middle right figure) and 5.4 days (bottom row figures), as calculated by Braithwaite and Nordlund (2006).

field will result in asymmetrical rotating. This will create a time varying quadrupole and consequently gravitational radiation.

The wave strain (h) resulting from such a configuration is fairly straightforward to calculate. We first calculate the moments of inertia (I). From there we can obtain a quantity known as ellipticity (ϵ), which is directly proportional to h.

$$\epsilon = \frac{I_{zz} - I_{xx}}{I_0} \tag{18}$$

$$I_{jk} = \int_V \rho(r)(r^2\delta_{jk} - x_j xk)dV \tag{19}$$

$$h = \frac{16\pi^2 G}{c^4}\frac{\epsilon I_0 f^2}{r} \tag{20}$$

Here, I_{xx} and I_{zz} are the moments of inertia with respect to the rotational and magnetic axes respectively.

Though we have observed 2,000 neutron stars in our Milky Way, our targets for gravitational wave emission are newly born stars. This is because they will have periods that correspond to detectable frequencies, unlike the magnetars we know of which have frequencies too low for LIGO to detect (below 10Hz). As these young stars emit gravitational radiation, they lose energy causing them to spin down below what LIGO can see.

2.3 Alfven Time

The Alfven crossing time is the time it takes for a magnetic wave to cross a star. This is the time scale that we are interested in for our simulations, as it is the time scale on which either the star will stabilize or our simulation will break down and no longer be able to run. It is straightforward to calculate the Alfven speed:

$$v_A = \frac{B_0}{\sqrt{\mu_0\rho_0}} \tag{21}$$

and from there the Alfven crossing time:

$$t_A = \frac{d}{v_A} \tag{22}$$

Noticing that $v_A \propto \frac{1}{\sqrt{\rho_0}}$, we see that waves will take infinite time to propagate in a vacuum. Thus, we can anticipate problems calculating with $\rho = 0$. It is critical to consider this when modeling a neutron star, as our code will have difficulty processing a perfect vacuum beyond the boundary of the star.

2.4 Magnetohydrodynamic Equations and Flux Freezing

To consider the problem of gravitational emission from a magnetic neutron star, it is important to be acquainted with the magnetohydrodynamic equations. The ideal MHD equations are below, which are composed of the HD equations and Maxwell's equations:

MHD Equations:

$$\frac{\partial \rho}{\partial t} + \nabla \cdot (\rho \vec{v}) = 0 \tag{23a}$$

$$P(\frac{\partial \vec{v}}{\partial t} + \vec{v} \cdot \nabla \vec{v}) + \nabla P - p\vec{g} - \frac{1}{\mu_0}(\nabla \times \vec{B}) \times \vec{B} = 0 \tag{23b}$$

$$\frac{\partial P}{\partial t} + \vec{v} \cdot \nabla P + \gamma P \nabla \cdot \vec{v} = 0 \tag{23c}$$

$$\frac{\partial \vec{B}}{\partial t} - \nabla \times (\vec{v} \times \vec{B}) = 0 \tag{23d}$$

$$\nabla \cdot \vec{B} = 0 \tag{23e}$$

These are a set of five partial differential equations describing the physical properties of plasma. These are particularly applicable to astrophysics and cosmology, as 99% of the baryonic matter content of the universe is made up of plasma.

From these equations, we can see mathematically how permanent magnetic field lines can become frozen into the crust of the star through a process known as "flux freezing". This concept is important to our discussion as it explains why magnetars can retain their high field strengths.

We begin with MHD Ohm's Law

$$\vec{E} + \vec{v} \times \vec{B} = 0 \tag{24}$$

Next we recall Faraday's Law:

$$\Phi = \int_S \vec{B} \cdot ds \tag{25}$$

Differentiating Faraday's Law in two parts and applying Stokes Theorem, we get:

$$(\frac{\partial \Phi}{\partial t}) = (\frac{\partial \Phi}{\partial t})_1 + (\frac{\partial \Phi}{\partial t})_2 \tag{26a}$$

$$(\frac{\partial \Phi}{\partial t})_1 = \int_S \frac{\partial \vec{B}}{\partial t} \cdot d\vec{s} = -\int_S \nabla \times \vec{E} \cdot d\vec{s} \tag{26b}$$

$$(\frac{\partial \Phi}{\partial t})_2 = \int \vec{B} \cdot \vec{v} \times \vec{dl} = \int \vec{B} \times \vec{v} \cdot \vec{dl} = \int \nabla \times (\vec{B} \times \vec{v}) \times d\vec{s} \tag{26c}$$

Combining our two equations back together, we find

$$(\frac{\partial \Phi}{\partial t}) = -\int_S \vec{E} + \vec{v} \times \vec{B} \cdot d\vec{s}. \tag{27}$$

Recalling that

$$\vec{E} + \vec{v} \times \vec{B} = 0 \tag{28}$$

we see,

$$\frac{\partial \Phi}{\partial t} = 0. \tag{29}$$

From this, we can determine that the flux remains constant at every contour, and thus the field lines move with the plasma. They are "frozen in"!

3 Methods and Results

3.1 PLUTO

"PLUTO is a freely-distributed software for the numerical solution of mixed hyperbolic/parabolic systems of partial differential equations (conservation laws) targeting high Mach number flows in astrophysical fluid dynamics. The code is designed with a modular and flexible structure whereby different numerical algorithms can be separately combined to solve systems of conservation laws using the finite volume or finite difference approach based on Godunov-type schemes. Equations are discretized and solved on a structured mesh that can be either static or adaptive"(PLUTO-cite better). PLUTO is a C based code employing the MHD equations.

A major drawback to PLUTO is that it does not solve the Poisson equation. Rather, the user is required

to manually enter in appropriate gravitational potentials. For instructions on how to set up PLUTO on a Mac computer, see Appendix 1.

For my work, PLUTO was used to model a stable neutron star as an n=1 polytrope, first in hydrostatic equilibrium and then with addition of magnetic fields. The code is used in conjunction with the program VisIT, which turns the numerical simulations into visualizations. We used a grid with 20 grid points in the radial, theta and phi directions for our simulations, to provide enough resolution to extract useful information, but still limit computing time.

3.2 Polytropes

Many stars are well modeled as polytropes, and thus are described by the polytropic equation of state:

$$P = K\rho^{1+1/n}. \tag{30}$$

We are interested in examining the stability of neutron stars over several Alfven time scales. To determine the initial conditions that will result in a stable star, we begin by considering a star in hydrostatic equilibrium, balancing $F_{Gravity}$ and $F_{Pressure}$.

$$\frac{dP(r)}{dr} = -\rho(r)\frac{Gm(r)}{r^2} \tag{31}$$

with

$$\frac{dm(r)}{dr} = 4\pi r^2\rho(r) \tag{32}$$

as the mass contained within radius r. Taking the divergence of equation 31 and plugging in equation 32, we obtain:

$$\frac{1}{r^2}\frac{d}{dr}(\frac{r^2}{\rho}\frac{d\rho}{dr}) = -4\pi G\rho \tag{33}$$

We insert our polytropic equation of state, and with the following change of variables:

$$r = \xi\alpha$$

$$\rho = \Theta^n\rho_c \tag{34}$$

$$where \quad \alpha^2 = K\frac{n+1}{4\pi G}\rho_c^{(1-n)/n}$$

This gives us a greatly simplified expression, known as the Lane-Emben Equation:

$$\frac{1}{\xi^2}\frac{d}{d\xi}(\xi^2\frac{d\Theta}{d\xi}) = -\Theta^n \tag{35}$$

with initial conditions $\Theta(0) = 1$ and $\Theta'(0) = 0$.

For the general case of an unspecified n, the Lane-Emden equation cannot be solved analytically and, rather, needs to be tackled numerically. For these instances, a numerical solver has been written in C for the equation, which employs the fourth-order Runge-kutta method. To use this, we break our second order differential equation into the following system of two first order equations:

$$\frac{d\Theta}{d\xi} = -\frac{z}{xi^2} \tag{36a}$$

$$\frac{dz}{d\xi} = \Theta^n \xi^2. \tag{36b}$$

We can rederive ρ and P from the results. The full code can be found in Appendix 2.

N=1 Polytrope

Neutron stars are best modeled as n=1 polytropes. Fortunately, the n=1 case of the lane-emden equation be solved analytically. We take

$$P = K\rho^2 \tag{37}$$

as our equation of state. Then, the Lane-Emden equation becomes

$$\frac{1}{\xi^2}\frac{d}{d\xi}(\xi^2\frac{d\Theta}{d\xi}) = -\Theta \tag{38}$$

We obtain as a solution

$$\Theta(\xi) = \frac{sin(\xi)}{\xi} \tag{39}$$

and returning to our original variables, find our initial conditions in ρ and P to be:

$$\rho(r) = \rho_c \frac{sin(\pi r/R)R}{r\pi} \qquad r < R \tag{40a}$$

$$P(r) = K\rho(r)^2 \tag{40b}$$

For a star of radius R=10km and mass M=1.4$M_\odot$, we obtain constants:

$$\rho_c = 2.2 * 10^{15} g/cm^3 \tag{41}$$

$$K = 4.25 * 10^4 g^{-1} cm^5 s^{-2} \tag{42}$$

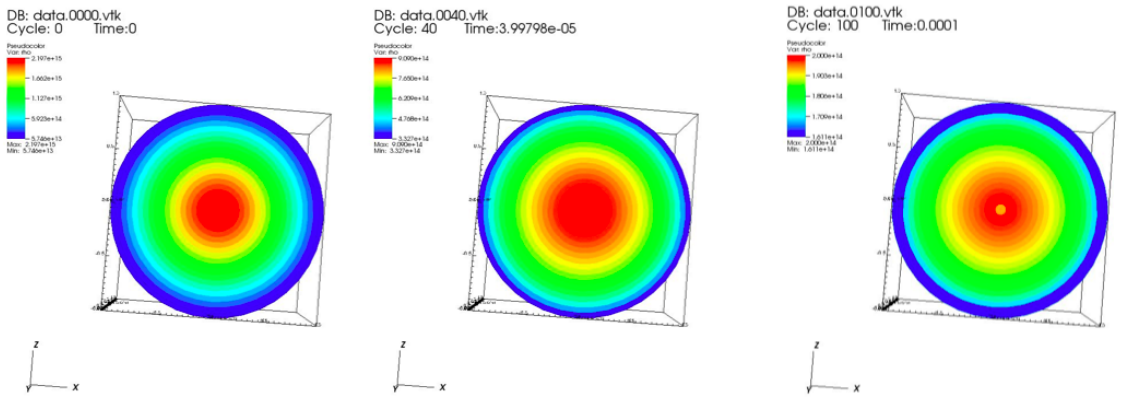

Figure 4: An evaporating polytrope.

Giving PLUTO solely these initial conditions will, as expected, result in a star that evaporates, as seen in figure 4.

This is a positive first result, for it allows us to see that the code is behaving how we expect.

The next step is to introduce an appropriate gravitational potential.

Gravitational Potential

To prevent the evaporation of our star, we need to introduce a gravitational potential. Giving PLUTO a large potential at random, in order to test the code and ensure it is working appropriately, we as expected find a collapsing star, as shown in figure 5.

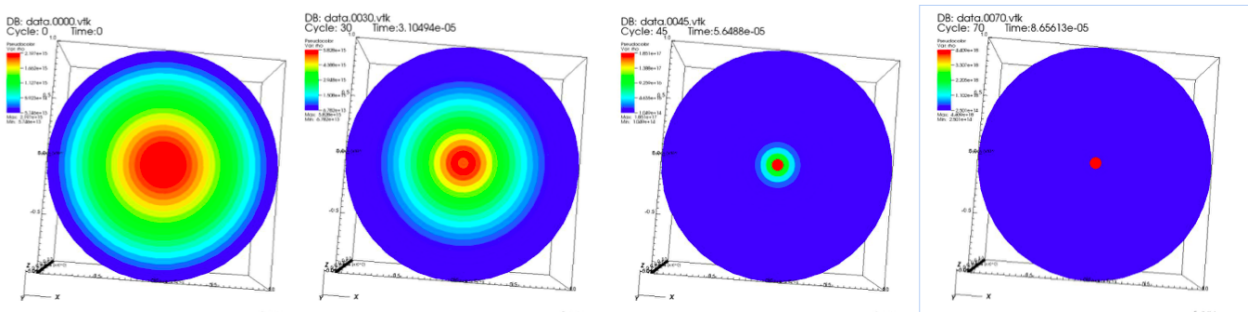

Figure 5: A collapsing polytrope

To find the appropriate potential for our n=1 polytrope, we begin with the Poisson equation.

$$\frac{1}{r^2}\frac{d}{dr}(r^2\frac{d}{dr}\phi) = 4\pi G\rho \tag{43}$$

PLUTO does not have the machinery to solve the Poisson equation, and thus it is our job to derive the gravitational potential and manually type it into the code. To do so, we recall our equation for density $\rho = \frac{\rho_c sin(\pi r/R)R}{r\pi}$, which we use in the Poisson equation to solve for the potential.

$$\phi = 4G\rho_c R \int \frac{dr}{r^2}[\int r sin(\pi r/R)dr] = 4G\rho_c(\frac{-R^3 sin(\pi r/R)}{\pi^2 r} + \frac{C_1}{r} + C_2) \tag{44}$$

with

$$\phi(0) = 0 \qquad \phi(R) = -\frac{GM}{R} \tag{45}$$

To avoid a singularity at R=0, we need to take C_1=0. Matching conditions at the boundary, we obtain C_2=$\frac{-M}{4R\rho_c}$. After solving for constants, we still have $\frac{1}{r}$ behavior at the center, which can be remedied by taking the limit of $\frac{sin(\pi r/R)}{r}$ as r approaches 0, which is $\frac{\pi}{R}$, and replacing it in our expression for ϕ_0. We now have our potential:

$$\phi_0 = 4G\rho_c(-\frac{R^2}{\pi}) - \frac{M}{4R\rho_c} \tag{46a}$$

$$\phi_{inside} = 4G\rho_c(\frac{-R^3 sin(\pi r/R)}{\pi^2 r} - \frac{M}{4R\rho_c}) \tag{46b}$$

$$\phi_{outside} = -\frac{GM}{r} \tag{46c}$$

3.3 Hydrostatic Equilibrium

With these initial conditions, we are able to model a neutron star (as an n=1 polytrope) in hydrostatic equilibrium.

Initial Conditions:

$$\rho(r) = \rho_c \frac{sin(\pi r/R)R}{r\pi} \qquad r < R \tag{47a}$$

$$P(r) = K\rho(r)^2 \tag{47b}$$

$$\phi_0 = 4G\rho_c(-\frac{R^2}{\pi}) - \frac{M}{4R\rho_c} \tag{47c}$$

$$\phi_{inside} = 4G\rho_c(\frac{-R^3 sin(\pi r/R)}{\pi^2 r} - \frac{M}{4R\rho_c}) \tag{47d}$$

$$\phi_{outside} = -\frac{GM}{r} \tag{47e}$$

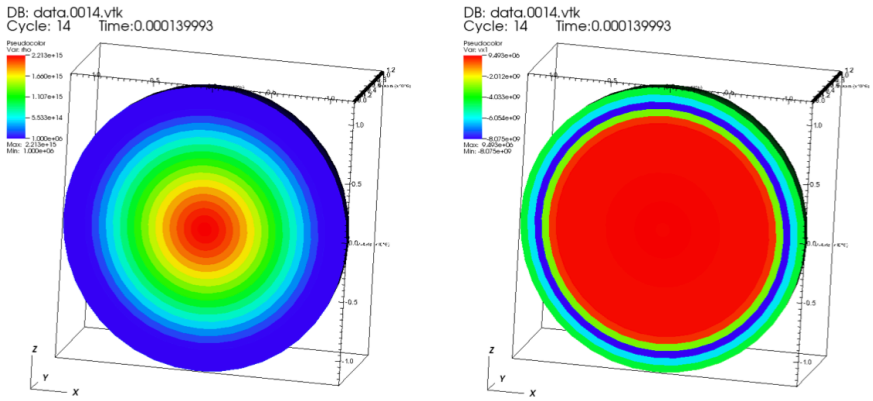

Figure 6: The density and velocity profiles, respectively, for a star in hydrostatic equilibrium

Through time scales of 1s in PLUTO, we see no changes beyond small oscillations in both the density and velocity profiles. The velocity profile makes sense physically: we expect some very slight movement in the interior that is essentially constant throughout.

Once our star is stable, we introduce a magnetic field.

3.4 Magnetic Field

As mentioned previously, for gravitational wave detection it is critical to understand the magnetic field configurations of stable stars. This will allow us to determine how they deform and, if rotating, what wave strain we can expect as a consequence. Though rotation is critical for the star to emit gravitational radiation, we will neglect its effects as they pertain to the magnetic field, in order to simplify our model and calculations. This is a reasonable approximation, as magnetars rotate slowly.

To construct a magnetic field, we closely follow the work of Haskell, Samuelsson, Glampedakis and Andersson 2008. We begin with the equation for magnetohydrostatic equilibrium.

$$\frac{\nabla\rho}{P} + \nabla\phi = \frac{(\nabla \times \vec{B}) \times \vec{B}}{4\pi\rho} = \frac{\vec{L}}{4\pi\rho} \tag{48}$$

Where $\vec{L}$ is the Lorentz force, and the gravitational potential ϕ obeys the Poisson equation. From Maxwell's equations, we know that,

$$\nabla \cdot \vec{B} = 0 \tag{49}$$

and that we are considering a barytropic equation of state, meaning $\rho = \rho(P)$. Taking the curl of equation

48, we get

$$\nabla \times [\frac{\vec{B} \times (\nabla \times \vec{B})}{\rho}] = 0 \tag{50}$$

which is a constraint our field must satisfy. Whichever field is arrived upon for the interior of the star must also match the exterior solution for a field:

$$\vec{B}_{ext} = \sum_{l \geq m} -(l+1)(\frac{A_l}{r^{l+2}} Y_l^m \hat{r} + \frac{A_l}{r^{l+2}} \partial_\theta Y_l^m \hat{\theta} + \frac{imA_l}{r^{l+2}} sin(\theta) Y_l^m \hat{\phi}) \tag{51}$$

We thus have constraints on our initial field configurations. We begin by exploring a purely poloidal field, using the dimensionless radius $y = \frac{\pi r}{R}$. Inside of the star, the magnetic field is described by:

$$\vec{B}_r = \frac{B_s cos(\theta)}{\pi(\pi^2 - 6)} [y^3 + 3(y^2 - 2) sin(y) + 6y cos(y)] \tag{52a}$$

$$\vec{B}_\theta = \frac{B_s sin(\theta)}{2\pi(\pi^2 - 6)} [-2y^3 + 3(y^2 - 2)(sin(y) - y cos(y))] \tag{52b}$$

$$\vec{B}_\phi = 0 \tag{52c}$$

where B_s is our maximum field strength. Taking $l = 1$, we obtain our conditions outside of the star:

$$\vec{B}_r = \frac{B_s R^3 cos(\theta)}{r^3} \tag{53a}$$

$$\vec{B}_\theta = \frac{B_s R^3 sin(\theta)}{2r^3} \tag{53b}$$

$$\vec{B}_\phi = 0. \tag{53c}$$

We use a maximum field strength of 10^{17}G, which is on the higher end of what we expect for these stars. This reduces our Alfven time and allows for simulations to complete more rapidly. When this is run without any rotation, no toroidal component develops and the code stops running after thirteen time steps. When a rotation of 10^6cm/s is introduced, the code can run for twice as long. We find, in this instance, that our poloidal field becomes unstable and the code can no longer run after 2.6×10^{-5} seconds. However, this is not before we see the development of a toroidal component, as the star works to stabilize. This is easily seen in figure 8. The configuration we see as part of figure 7 (before the code stops), in which we have a tightly wound coil within the boundary of the star and a dipole field outside is, very generally, what we expect in a stable star.

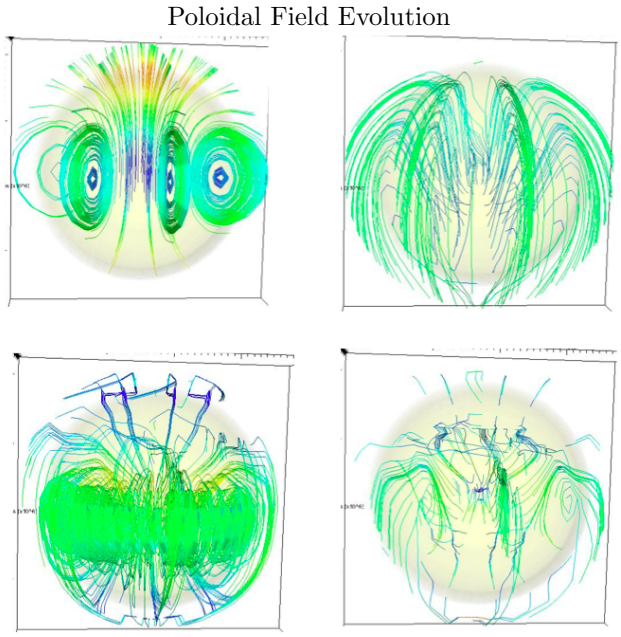

Figure 7: A poloidal field (with rotation) of maximum strength B=10^{17} G at t=0s (top left), $9 \times 10^{-6} s$ (top right), $2.3 \times 10^{-5} s$ (bottom left), and $2.6 \times 10^{-5} s$ (bottom right). The final configuration is within a time step (10^{-8}s) of when the code crashes.

We also explore the evolution of an initially toroidal magnetic field: Inside star:

$$\vec{B}_r = 0 \tag{54a}$$

$$\vec{B}_\theta = 0 \tag{54b}$$

$$\vec{B}_\phi = \frac{B_s sinysin\theta}{\pi} \tag{54c}$$

$$\tag{54d}$$

Outside star:

$$\vec{B}_r = 0 \tag{54e}$$

$$\vec{B}_\theta = 0 \tag{54f}$$

$$\vec{B}_\phi = 0. \tag{54g}$$

We again take a maximum field strength of $B_s = 10^{17}$G. Our field rapidly develops a poloidal component within the first time step ($10^{-8} s$), and proceeds to a twisted torus configuration over long time scales, as

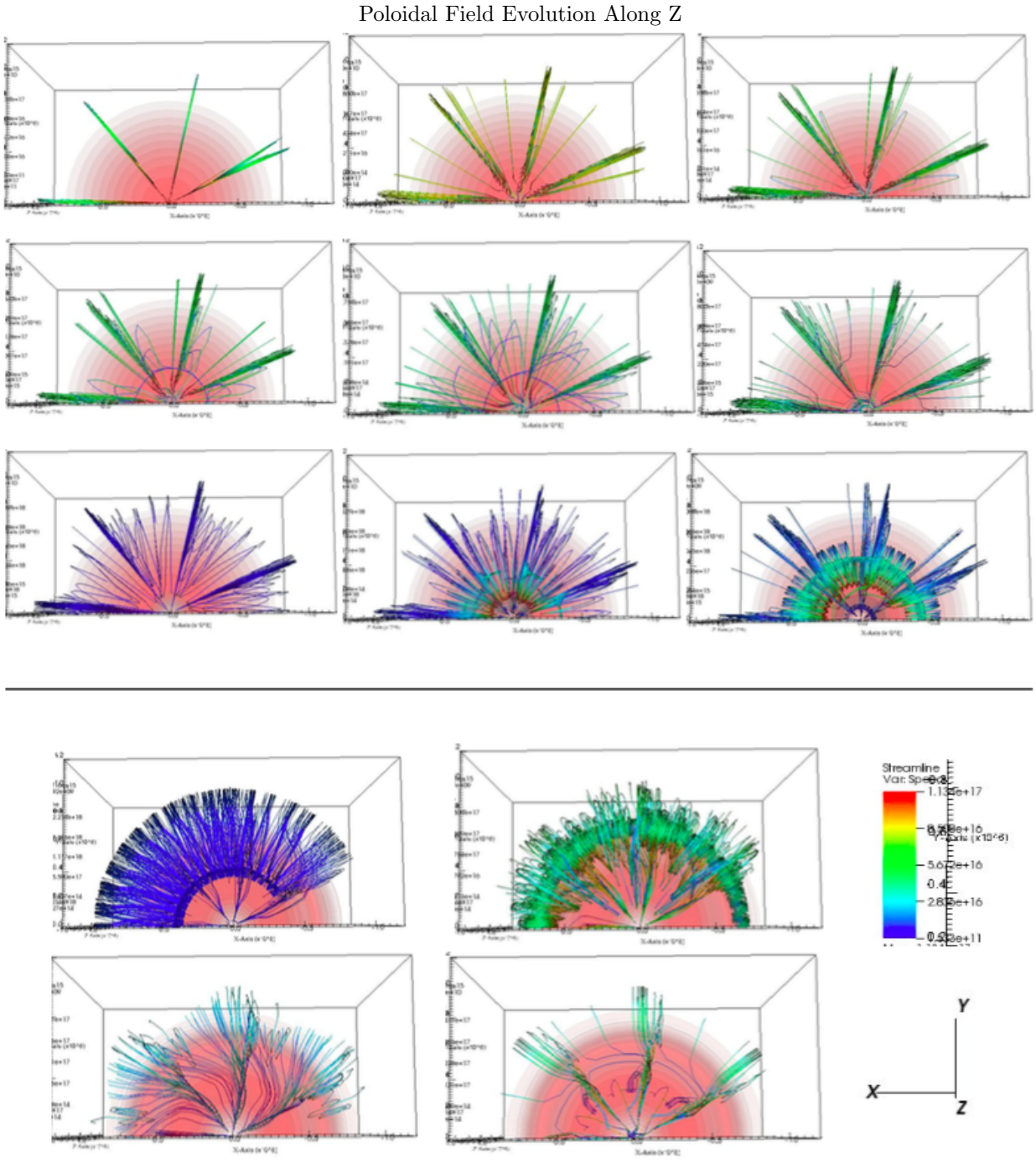

Figure 8: We see the development of a toroidal component in an initially poloidal field (with rotation), as well as the formation of a coil like structure that is typical of fields in stable stars. These snapshots span from t=0 s to t=2.6×10^{-5} s. The top figures are snapshots between equal time intervals of 10^{-8}, while the bottom figures are interesting configurations that arise throughout the evolution. The final two figures on the bottom are just before the code ceases running, and show the deterioration of a promising field structure.

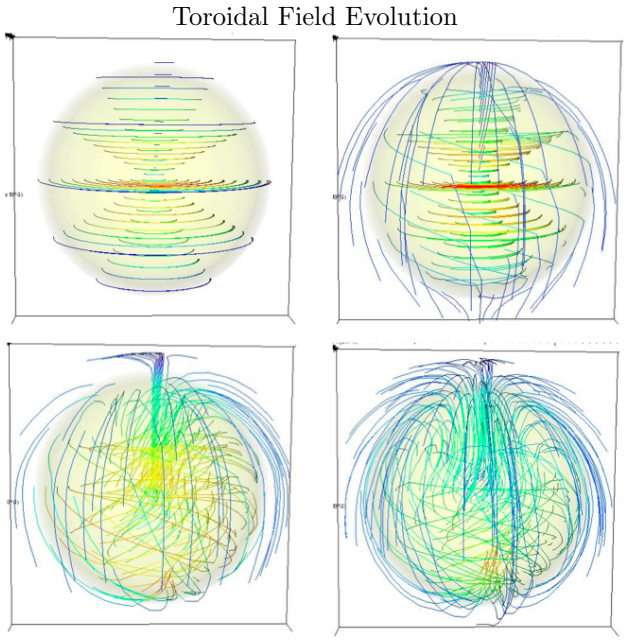

Figure 9: The evolution of a toroidal field of maximum strength B=10^{17}, at times t=0s (top left), 1×10^{-4}s (top right), 5×10^{-3}s (bottom left), and 10^{-2}s (bottom right).

seen in Figure 9. We have run this simulation for 10^{-2}s, and thus far it has been stable. Integrating both our toroidal and poloidal components over the volume separately after 100 time steps reveals them to be approaching each other in magnitude: $B_T = 5.22 \times 10^{15}$ and $B_P = 6.51 \times 10^{1}5$. This is an encouraging sign, as we know from Braithwaite's work that stable fields require toroidal and poloidal components that are nearly equal in magnitude.

When simulating in PLUTO, we must make the unphysical approximation of giving the vacuum outside of the star a density. This is because, as we know from our previous discussion of time scales, when we have a magnetic field in a vacuum we will be dividing my zero for our time. Thus, without a field of 10^{1}0G on the exterior of the star, our code will stop running almost immediately. While this approximation does prevent our model from being entirely realistic, it is fair, as the interior of the star is still more dense by five orders of magnitude than the outside.

3.5 Gravitational Wave Strain

It is now time to asses the magnetars we have simulated for their potential to generate detectable gravitational radiation. Earlier, we discussed the methodology for calculating wave strain(h) when the magnetic and rotational axes are nonaligned, via moment of inertia (I) and ellipticity (ϵ)

$$\epsilon = \frac{I_{zz} - I_{xx}}{I_0} \tag{55}$$

$$I_{jk} = \int_V \rho(r)(r^2\delta_{jk} - x_j xk)dV \tag{56}$$

$$h = \frac{16\pi^2 G}{c^4}\frac{\epsilon I_0 f^2}{r}. \tag{57}$$

Recall that the moment of inertia of a solid sphere is:

$$I = \frac{2}{5}MR^2. \tag{58}$$

While it takes a rotating star, with the rotational axis offset from the magnetic axis, to produce gravitational radiation in reality, a calculation with the aligned axes, which is a significantly simpler simulation, should be sufficient for our purposes. Thus, this is what we have carried out in the prior calculations in this paper. Evidently, we need a modification to the wave strain if the two axes are aligned, as $I_{zz} - I_{xx} = 0$. We can approximate the deformations in a star with aligned axes for both the poloidal and toroidal fields to first order, as follows.

Poloidal Field:

$$\epsilon_P = -10^{-10}(\frac{R}{10km})^2(\frac{M}{1.4M_\odot})^{-2}(\frac{B}{10^{12}G})^2 \tag{59a}$$

Toroidal Field:

$$\epsilon_T = -10^{-12}(\frac{R}{10km})^4(\frac{M}{1.4M_\odot})^{-2}(\frac{B}{10^{12}G})^2 \tag{59b}$$

We consider the two components separately, as they deform the star in different ways.

Rotation is also neglected in our model. This is a fair approximation, as magnetars spin very slowly. Even in the more rapidly rotating strongly magnetized newborn neutron stars, which we investigate, if we

do not have differential rotation, the topology of the surface will hardly be changed (though the growth of instabilities will be affected), and we can continue using our approximation.

We can use VisIT to integrate our magnetic field over the star, allowing us to calculate the ellipticity for both cases we have simulated. To do this, we must separately define expressions within visit for the magnitude of both the toroidal and poloidal components divided by the overall star volume. Because we are doing integration over a spherical surface, we must multiply both by $r^2 sin\theta dr d\theta d\phi$. We manually calculate and enter into our expression $dr d\theta d\phi$, by considering our box size and grid size. We have 20 radial points spanning a 1.2×10^6 radius, and 20 angular points spanning 2π and pi degrees in θ and ϕ. Thus, our dV=$\frac{1.2\times10^6}{20}\frac{2\pi}{20}\frac{\pi}{20} \approx 3,000$. We obtain for our ellipticity:

At Time Step 0

$$\epsilon_{poloidal} = 0 \tag{60a}$$

$$\epsilon_{toroidal} \ -2 \times 10^{-4} \tag{60b}$$

At Time Step 100

$$\epsilon_{poloidal} \ -3.6 \times 10^{-3} \tag{60c}$$

$$\epsilon_{toroidal} \ -2.5 \times 10^{-5}. \tag{60d}$$

This tells us that the type of deformation changes, as our star goes from stretched to squeezed.

Calculating wave strain is, again, trivial if one knows the period of the star and its distance away. While we do not have this information, we can investigate the distances at which a magnetar spinning with a set frequency can produce detectable signals. We know LIGO requires h$\geq 10^{-23}$. Considering ϵ after 100 time steps, with some simple algebraic manipulation we see that for a frequency of 10Hz (the lower bound of what LIGO can detect), a star with this field strength and configuration can be detected at roughly 530 light years from Earth. For a frequency of 100Hz, the wave strain will be adequate if the star is at a distance of roughly 53,000 light years.

The accuracy of these calculations is restricted by our grid size, which has 20 radial and angular points.

However, our results should be sufficient for this investigation.

4 Conclusion

Our simulations and calculations of wave strain reveal that newly born, rapidly rotating and strongly magnetised neutron stars are a promising source for gravitational wave detectors such as LIGO.

From here, there is still much work to be done. In the short term, running the same simulations with higher grid resolution will help improve the ellipticity and consequently wave strain calculations. Then, adding rotations, investigating different axial separations and considering temperature in the equation of state will all contribute to the accuracy of our model. We might also consider a variety of field configurations, and calculate the ellipticity directly.

Works Cited

"All You Need to Know about Gravitational Waves." *Nature.com*. Nature Publishing Group, Mar. 2014. Web. 27 Apr. 2015.

Braithwaite, J., and Å. Nordlund. "Stable Magnetic Fields in Stellar Interiors." Astronomy and Astrophysics A&A 450.3 (2006): 1077-095. Web.

Braithwaite, J., and H. C. Spruit. "Evolution of the Magnetic Field in Magnetars." Astronomy and Astrophysics A&A 450.3 (2006): 1097-106. Web.

Braithwaite, J. "The Stability of Toroidal Fields in Stars." Astronomy and Astrophysics A&A 453.2 (2006): 687-98. Web.

Braithwaite, Jonathan, and Hendrik C. Spruit. "A Fossil Origin for the Magnetic Field in A Stars and White Dwarfs." Nature 431.7010 (2004): 819-21. Web.

Carroll, Sean M. *Spacetime and Geometry: An Introduction to General Relativity*. San Francisco: Addison Wesley, 2004. Print.

Chapter 9: The MHD Kinematic Mean Field α2-dynamo." *Nonconservative Stability Problems of Modern Physics* (2013): n. pag. Web.

"Gravitational Waves Detected." *Science News* 95.25 (1969): 593-94. Web.

"Gravitational Waves." *Gravitational Waves*. Caltech, n.d. Web. 27 Apr. 2015.

Hartle, James. *Gravity*. N.p.: n.p., 2002. Print.

Https://www.advancedligo.mit.edu/. N.p., n.d. Web.

Haskell, B., L. Samuelsson, K. Glampedakis, and N. Andersson. "Modelling Magnetically Deformed Neutron Stars." Monthly Notices of the Royal Astronomical Society 385.1 (2008): 531-42. Web.

Haskell, Brynmor. "Gravitational Waves from Deformed Rotating Neutron Stars." Thesis. University of Southhampton, 2006. Print.

Jaranowski, Piotr, Andrzej Królak, and Bernard F. Schutz. "Data Analysis of Gravitational-wave Signals from Spinning Neutron Stars: The Signal and Its Detection." Physical Review D Phys. Rev. D 58.6 (1998): n. pag. Web.

Appendix 1: PLUTO Installation

Two things need to be installed before PLUTO is usable: Python and GNUMake. Python is the easier one to install: The most recent version can be downloaded from their website. GNUMake is a bit harder to install. Download the file from their website http://ftp.halifax.rwth-aachen.de/gnu/make/ (mine was called make-4.1.tar.gz) and install it. Find the folder in downloads, unzip it, and look at the INSTALL document for installation instructions.

If while installing you get a permission denied error, as I did, try instead,

$sudo make install

Now, this actually didnt work for me it said I didnt have something called autoconf.

If you get an error anywhere in the above text and it says you dont have autoconf, do as follows: Autoconf requires two others to work: Perl, and m4. Perl is already installed on macs, but you will need to get m4. Go to ftp://ftp.gnu.org/gnu/m4/ and choose m4-1.4.tar.gz. The installation process should be quite similar to the one for GNUMake, with instructions in another INSTALL file.

Once these steps are complete, autoconf needs to be installed. It can be found on the site http://ftp.gnu.org/gnu/autoconf/ where you should choose autoconf-latest.tar.gz from the bottom, and install it. Autoconf should now be installed. Now just repeat the GNUMake installation steps.

When you downloaded Pluto, you should have gotten a file called pluto-4.1.tar.gz. Unzip it. Pluto is less clear when it comes to installationyoull have to do some file moving to make it work. The following steps are a condensed version of the README file in the PLUTO folder.

Steps for installing PLUTO:

Open up finder, and go to your downloads folder. Copy the PLUTO folder. It needs to be pasted into your specific Users folder, which is accessed through Macintosh HD. In the Users folder (within Macintosh HD), one of the icons should be your current user account, probably called your name. Mine has a little house as an icon. Click on whatever account is the one you are using. Then paste in your PLUTO folder. Now, you need to make a working directory, which is easiest to do in your specific Users folder. This will be where all of your PLUTO files get saved. Open up the terminal and navigate to this folder. Then do the following

$export PLUTO_DIR=/Users/name/PLUTO except, obviously, with the name of your user account instead

of "name". Again, this is the name of the folder that we pasted the PLUTO folder into. It is case sensitive, so be sure to pay attention to capitalization. This command just defines the term PLUTO_DIR so the program knows where all the PLUTO program files are located. Once youve done that, you can do $python $PLUTO_DIR/setup.py

Once you hit enter, it should open up PLUTO's terminal interface. If you get here then PLUTO has successfully been installed!

To obtain our simulations, some alterations had to be made within PLUTO. The square of the sound speed, which is related to the equation of state by ${c_{sound}}^2 = 2P/\rho$, had to be modified in both the eos.c and fluxes.c files for an isothermal equation of state. In globals.h, γ needed to be modified from 5/3 to 2.

Appendix 2: Lane-Emden Solver

```
#include<stdio.h>

#include <math.h>


int main(){

float x,y,z,h,z1,z2,z3,z4,y1,y2,y3,y4,dx,n;

printf("Give n:\n");

scanf("%f",&n);

h=.0005;

dx=h;

z1=z2=z3=z4=y1=y2=y3=y4=0;

y=1.0;

z=0.0;

x=0.01;

FILE *NPolytrope;

NPolytrope = fopen("NPolytrope.dat", "w");

while(x<=3.14159)

{

y1 = h*z;

z1 = h*-1*pow(x,-2)*(2*x*z + pow(x,2)*pow(y,n));

y2 = h*(z+z1/2);

z2 = h*-1*pow(x+dx/2,-2)*(2*(x+dx/2)*(z+z1/2) + pow(x+dx/2,2)*pow(y+y1/2,n));

y3 = h*(z+z2/2);

z3 = h*-1*pow(x+dx/2,-2)*(2*(x+dx/2)*(z+z2/2) + pow(x+dx/2,2)*pow(y+y2/2,n));

y4 = h*(z+z3);

z4 = h*-1*pow(x+dx,-2)*(2*(x+dx)*(z+z3) + pow(x+dx,2)*pow(y+y3,n));
```

```
y = y+(y1+2*y2+2*y3+y4)/6;

z = z+(z1+2*z2+2*z3+z4)/6;

x = x+dx;


fprintf(NPolytrope,"%f\t %f\t %f\t %f\n",x,y,z,sin(x)/x);

}

return(0);

}
```